Mechanical Systems and Signal Processing 156 (2021) 107672

Contents lists available at ScienceDirect

Mechanical Systems and Signal Processing

journal homepage: www.elsevier.com/locate/ymssp

Achieve frequency-self-tracking energy harvesting using a passively adaptive cantilever beam

Chunbo Lan [a,*], Zhenning Chen [a], Guobiao Hu [b], Yabin Liao [c], Weiyang Qin [d]

[a] State Key Laboratory of Mechanics and Control of Mechanical Structures, Nanjing University of Aeronautics and Astronautics, Nanjing, PR China
[b] Department of Mechanical Engineering, University of Auckland, New Zealand
[c] Department of Mechanical Engineering Technology, Penn State Erie, the Behrend College, USA
[d] Department of Engineering Mechanics, Northwestern Polytechnical University, Xi'an, PR China

ARTICLE INFO

Article history:
Received 19 June 2020
Received in revised form 13 January 2021
Accepted 19 January 2021
Available online 2 February 2021

Keywords:
Passive self-adaptation
Piezoelectric energy harvesting
Frequency-tracking
Mode shape reconstruction
Cantilever beam with sliding mass

ABSTRACT

The frequency of the vibration in the ambient environment varies frequently, which imposes a great challenge for robust energy harvesting. To maintain the high performance of harvesting the variant-frequency vibration, one efficient means is to make the energy harvester track the excitation frequency by itself. To obtain a frequency-self-tracking (FST) energy harvester, an interesting system, e.g., the passively self-adaptive structure, has attracted a lot of attention recently. Though passively self-adaptive systems designed based on symmetric structures have been considerably reported, the passive self-adaptation of asymmetric structures is still an open question to be explored. To this end, this paper investigates the dynamics of a cantilever beam with a sliding mass. Experimental results indicate that the passively self-adaptive behavior occurs in the second eigenmode rather than the fundamental eigenmode, which is essentially different from the symmetric structures reported in the existing literature. The proposed FST system can self-adjust its natural frequency to match the excitation frequency and achieve large response without any external manual intervention, showing a promising potential to attain high-efficient energy harvesting from variant-frequency vibration. Therefore, this novel passive self-adaptation behavior is employed for piezoelectric energy harvesting. By introducing a piezoelectric transducer, an FST vibration energy harvester (VEH) is achieved. Owing to the passive self-adaptation capability, the proposed FST-VEH exhibits a significantly enhanced energy harvesting performance over a wide range of frequency and an increase of the output voltage amplitude for more than 800%. In general, the proposed FST-VEH demonstrates a great potential to make a significant breakthrough in harvesting variant-frequency vibration energy.

1. Introduction

Vibration energy harvesting, which is regarded as a promising sustainable energy solution for micro-electromechanical devices, has been extensively developed during the past few decades [1–8]. The environmental vibration often exists over a broadband spectrum. It is featured with the time-varying characteristic, imposing a big challenge on the conventional linear vibration energy harvester (VEH): how to enlarge the operation bandwidth and maintain the high efficiency. To deal with

* Corresponding author.
E-mail address: chunbolan@nuaa.edu.cn (C. Lan).

https://doi.org/10.1016/j.ymssp.2021.107672
0888-3270/

these problems, nonlinearity [9–15] has been introduced into vibration energy harvesting systems, such as Duffing-type VEHs [9–19] nonlinear 2-DOF VEH [13] internal resonance-based VEH [14] impact-based VEH [15] etc. To name a few, Stanton *et al.* [9] developed a nonlinear monostable VEH using magnets and found that it has a wider bandwidth and larger output power than its linear counterpart. Erturk *et al.* [10] found that the inter-well oscillation of a bistable VEH could not only largely increase the output power but also significantly broaden the bandwidth. Zhou *et al.* [11] investigated a tristable VEH, and experimentally demonstrated that it was very suitable for harvesting energy from human motion. Liu *et al.* [12] proposed an impact engaged VEH with mechanical stoppers as another efficient means for broadband energy harvesting. Chen *et al.* [13] designed an internal resonance energy harvester with a double jump phenomenon for achieving a significantly widened bandwidth.

On the foundation of the in-depth understanding of these nonlinear VEHs, it has been unveiled that when the excitation frequency varies or a small perturbation takes place, the aforementioned nonlinear VEHs may fall into the low-energy orbit from the high-energy orbit, resulting in the reduction of the output power and the decrease of the bandwidth [20]. To obtain high-energy orbit oscillations [21–29] the mechanical impact method [21] and the electrical method [25–29] have been developed in recent few years. Though a mechanical impact can trigger the high-energy orbit oscillations, an additional mechanical force is required in this process, which makes this method impractical for micro-scale applications [21]. From the application perspective, the electrical method is more physically implementable. However, the electrical method [25–29] consumes a certain amount of electric energy during operation, which could unfavorably deteriorate the energy efficiency.

As an unique and interesting system, the passively self-adaptive oscillator can autonomously adjust its natural frequency to match the excitation frequency without any manual intervention. It is very promising to solve the problem induced by the change of excitation frequency. However, the experimentally validated passively self-adaptive structures are still limited in the existing literature [30–36]. Boudaoud *et al.* [30] observed that a vibrating soap film could maintain a large-amplitude vibration over a wide frequency range since it could self-arrange the liquid distribution and autonomously achieve resonance according to the excitation. Brazovskaia *et al.* [31] experimentally studied the vibration of a smectic film carrying a mass. They found that the whole system can achieve resonance from 370 Hz to 670 Hz owning to the sliding mass. Similar self-adaptation phenomena in a string with sliding mass and a fixed–fixed beam with sliding mass were discovered by Boudaoud *et al.* [32] and Miller *et al.* [33] respectively.

Interestingly, it is noteworthy that all these self-adaptive structures reported in the existing literature [30–36] including the soap film [30] the smectic film with movable mass [31] the fixed-fixed string/beam with sliding mass [32–36] are all symmetric. Therefore, questions naturally arise here: does the self-adaptive phenomenon only occur in symmetric structures? If the self-adaptive phenomenon can also occur in asymmetric structures, does it have the potential to generate new possibilities for energy harvesting? With the curiosity to these unknowns, we are motivated to explore the passive self-adaptation in an asymmetric structure. The cantilever beam is one of the most representative asymmetric structures that has been widely used in designing linear and nonlinear piezoelectric energy harvester. Hence, achieving the passive self-adaptation in a cantilever beam is of great interest to deal with the variant-frequency energy harvesting problem. Therefore, the asymmetric structure investigated in this paper is a cantilever beam with a sliding mass. Notably, for the system of a cantilever beam with a sliding mass, Kaplan *et al.* [37] used various control methods to actively adjust the movable mass position so that the resonance frequency can be actively tuned to match the excitation frequency. In their study, active control methods are applied to realize the tuning operation. The whole system, including the auxiliary control system, is relatively complicated. Moreover, the active control process consumes additional energy, resulting in a decrease of the energy harvesting efficiency. In this paper, we focus on exploring the passive self-tuning behavior of a cantilever beam with a sliding mass. The whole system consists of a mass and a piezoelectric cantilever beam only. No control system is employed to tune the mass or other components.

The rest of this paper is arranged as follows. Section 2 describes the physical prototype and working principle of the proposed FST-VEH. Section 3 presents the mathematical modeling and the theoretical method to calculate the eigenfrequency and mode shape of the beam-mass system. Section 4 studies the passively self-adaptive behavior of the proposed system. Section 5 investigates the mode shape reconstruction characteristics of the cantilever-beam-mass system and evaluates its energy harvesting performance as compared with the conventional VEH. Several useful conclusions are given in Section 6.

2. Physical prototype, experimental setup and working principle

2.1. Physical prototype and experimental setup of FST-VEH

The fabricated physical prototype of the passively self-adaptive VEH, depicted in Fig. 1(a), consists of a sliding mass that can move along a cantilever beam. A piezoelectric transducer (MFC, M2814-P2) is bonded at the root of the cantilever beam and shunted to an external load resistance (R = 100 kΩ). Its output voltage is measured by a data acquisition system (DH5922D). Both the cantilever beam and the sliding mass are made of stainless steel. The width, thickness, and length of the cantilever beam are b = 10 mm, h_b = 0.5 mm, and l_b = 15.7 mm, respectively. The cantilever beam threads through the sliding mass with a rectangular opening of a height h_r. The width of the rectangular opening b_r = 10.2 mm is intentionally designed to be a bit wider than that of the cantilever beam to avoid getting stuck due to the width restrain. The detailed geometric dimensions of the system are annotated in Fig. 1(b). The cantilever beam is mounted on a 3D-printed fixture.

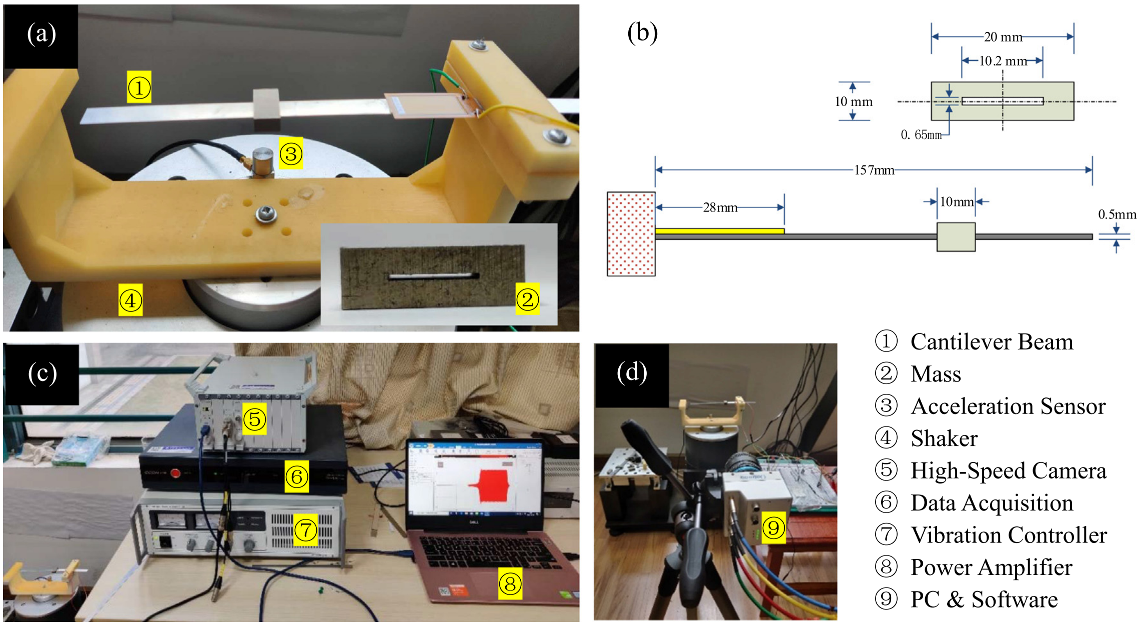

Fig. 1. Experimental setup: (a) self-adaptive energy harvester; (b) The dimension of the proposed FST-VEH; (c) vibration test and data acquisition equipment; (d) high-speed camera.

The whole system is installed to a 500 N electromagnetic shaker (E-JZK-50), which can simulate a vertical base excitation controlled at a constant acceleration level.

Fig. 1(c) and (d) show the experimental setups, including the high-speed camera, the controller, the amplifier, and the data acquisition system. The excitation frequency can be adjusted through interacting with the GUI interface of the software that communicates with the controller. The vibration controller (VT-9008), together with a feedback accelerometer, forms a closed-loop to guarantee the base excitation at the desired acceleration level. The power spectral density is kept constant in the experiment. The signal generated by the controller is amplified by the amplifier (E5874A) and then fed to the shaker for generating the excitation. The output voltage of the piezoelectric transducer is measured and recorded by a DATA acquisition system (DH5922D) with the sampling frequency of 2000 Hz. A high-speed camera (AcutEye-4M-500CXP), as shown in Fig. 2(b), is utilized to capture the trajectory of the sliding mass along the cantilever beam. Considering that the base excitation frequency varies from 60 Hz to 85 Hz in the experiment, the high-speed camera sampling frequency is set to be 500 Hz to guarantee its capability to identify the vibrating shape of the cantilever beam.

2.2. Working principle of FST-VEH

The working principle of the proposed frequency-self-tracking energy harvester (FST-VEH) is depicted in Fig. 2. We consider a circumstance under which the frequency of the external vibration source varies. If the excitation frequency f_1 is within the self-adaptive frequency range but different from the second eigenfrequency of the system at the initial state f_n ($f_n \neq f_1$), the mass will self-tune its location to reconstruct the 2nd mode shape of the beam. The mass stops sliding until arriving at a specific place, where the corresponding second eigenfrequency matches the excitation frequency, resulting in a large amplitude response. If the excitation frequency changes to f_2, the mass will self-slide to a new position, and the system can adjust its second eigenfrequency to match the excitation frequency f_2 for achieving a large amplitude response again. Thus, the system can self-track the excitation frequency without any manual intervention to maintain the large amplitude response even when the excitation frequency varies with the time. Hence, the proposed FST-VEH is designed to attain a robust energy harvesting capability in response to the excitation frequency change.

Notably, the passive self-adaptation in a cantilever beam with sliding mass takes place in the 2nd-order mode rather than the fundamental mode in our experimental results. In the fundamental mode, the mass always slides to the free end and eventually falls off.

3. Governing equations and eigenfrequency analysis of FST-VEH

3.1. Governing equations

As shown in Fig. 3, the proposed FST-VEH consists of a cantilever beam with a sliding mass. In comparison with the fixed–fixed beam with a sliding mass proposed by Miller *et al.*[33–34] the main difference between these two systems is the

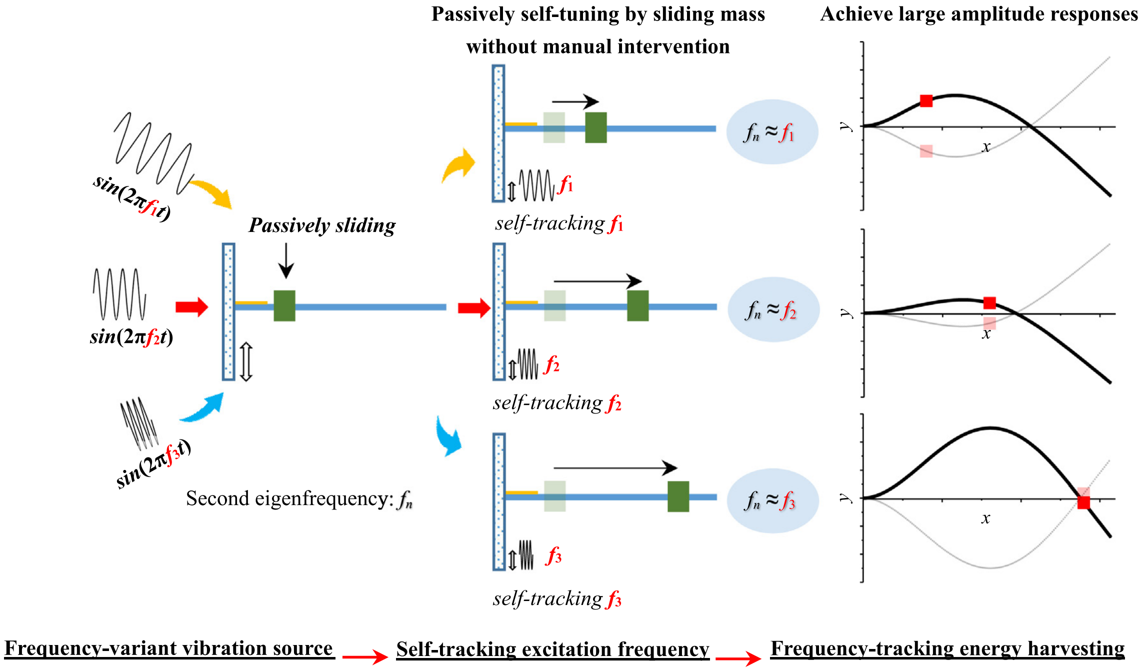

Fig. 2. Schematic illustration of the frequency-self-tracking energy harvesting through the passively self-adaptation of a cantilever beam with sliding mass.

boundary condition. Thus, the generic model of the beam-slider system proposed by Miller, *et al.*[33–34] can be employed in modeling the cantilever-mass system proposed in this paper. The governing equation of the proposed cantilever-mass system can be given as

$$
\begin{aligned}
&\rho A\left(\ddot{W}_0+\ddot{W}\right)+m\left(\ddot{W}_0+\ddot{W}+2\dot{W}'\dot{s}+W''\dot{s}^2\right)\delta(X-s)+EIW''''\\
&-\tfrac{d}{dX}\left[I_m\left(\ddot{W}'+2W''\dot{s}+W'''\dot{s}^2+W''\ddot{s}\right)\delta(X-s)\right]=0\\
&m\ddot{s}+m\left(\ddot{W}_0+\ddot{W}+2\dot{W}'\dot{s}+W''\dot{s}^2+W'\ddot{s}\right)W'+I_m\left(\ddot{W}'+2W''\dot{s}+W'''\dot{s}^2+W''\ddot{s}\right)W''=0
\end{aligned}
\tag{1}
$$

where ρ, A and I_m are the density, the cross-sectional area, and the moment of inertia of the mass, respectively. m is the weight of the sliding mass. E and I are the young's modulus and the moment of inertia of the beam, respectively. W_0 is the base displacement. A point along the beam is denoted by the coordinate X. $W(X, t)$ is the vertical displacement of the beam. The horizontal position and vertical position of mass are $s(t)$ and $W(s(t), t)$, respectively. The overdot denotes the time derivative. Notably, the collision-sliding behavior of the mass and the piezoelectric transducer are not considered in this model.

3.2. Eigenfrequency analysis

To study the passive self-adaptation of the proposed FST-VEH, the eigenfrequency and mode shape of the whole system should be obtained by assuming the mass location is fixed. For a cantilever beam with a fixed mass, the eigenfrequency and model shape can be analytically obtained by using the method in Ref. [34] and [38].

The modal shape of this system is assumed to be

$$
\Phi(X)=\begin{cases} a\cos(\beta X)+b\sin(\beta X)+c\cosh(\beta X)+d\sinh(\beta X), X<s \\ e\cos(\beta(X-s))+f\sin(\beta(X-s))+g\cosh(\beta(X-s))+h\sinh(\beta(X-s)), X>s \end{cases}
\tag{2}
$$

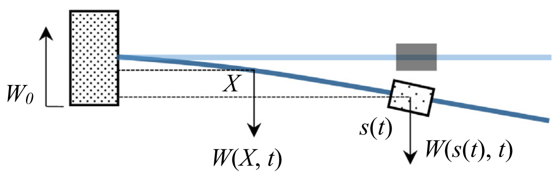

Fig. 3. Schematic of the cantilever beam with a sliding mass.

where

$$\beta = \sqrt[4]{\omega^2 \frac{\rho A}{EI}} \tag{3}$$

There are eight unknown coefficients in Eq. (2). Hence, we should find eight boundary conditions to solve these coefficients. The first four boundary conditions are the boundary conditions of the cantilever beam, which are given by

$$\Phi(0) = 0, \frac{d\Phi(0)}{dX} = 0, \frac{d^2\Phi(L)}{dX^2} = 0, \frac{d^3\Phi(L)}{dX^3} = 0 \tag{4}$$

The last four boundary conditions are the continuity conditions at the mass position, which are

$$\begin{cases} \Phi^-(s) = \Phi^+(s) \\ \frac{d\Phi^-(s)}{dX} = \frac{d\Phi^+(s)}{dX} \\ \frac{d^2\Phi^-(s)}{dX^2} = \frac{d^2\Phi^+(s)}{dX^2} \\ EI\frac{d^3\Phi^-(s)}{dX^3} - EI\frac{d^3\Phi^+(s)}{dX^3} = -m\omega^2\Phi(s) \end{cases} \tag{5}$$

Substituting the assumed mode shape Eq. (2) into the boundary conditions Eq. (4) and continuity conditions Eq. (5) yields

$$\begin{cases} a + c = 0 \\ b + d = 0 \\ -e\beta^2\cos(\beta(L-s)) - f\beta^2\sin(\beta(L-s)) + g\beta^2\cosh(\beta(L-s)) + h\beta^2\sinh(\beta(L-s)) = 0 \\ e\beta^3\sin(\beta(L-s)) - f\beta^3\cos(\beta(L-s)) + g\beta^3\sinh(\beta(L-s)) + h\beta^3\cosh(\beta(L-s)) = 0 \\ a\cos(\beta s) + b\sin(\beta s) - a\cosh(\beta s) - b\sinh(\beta s) = e + g \\ -a\sin(\beta s) + b\cos(\beta s) - a\sinh(\beta s) - b\cosh(\beta s) = f + h \\ -a\cos(\beta s) - b\sin(\beta s) - a\cosh(\beta s) - b\sinh(\beta s) = -e + g \\ a\beta^3\sin(\beta s) - b\beta^3\cos(\beta s) - a\beta^3\sinh(\beta s) - b\beta^3\cosh(\beta s) + f\beta^3 - h\beta^3 + \frac{m\omega^2}{EI}e + \frac{m\omega^2}{EI}g = 0 \end{cases} \tag{6}$$

Based on the first two expressions in Eq. (6), the above equations can be simplified as

$$\begin{cases} -\beta^2\cos(\beta(L-s))e - \beta^2\sin(\beta(L-s))f + \beta^2\cosh(\beta(L-s))g + \beta^2\sinh(\beta(L-s))h = 0 \\ \beta^3\sin(\beta(L-s))e - \beta^3\cos(\beta(L-s))f + \beta^3\sinh(\beta(L-s))g + \beta^3\cosh(\beta(L-s))h = 0 \\ [\cos(\beta s) - \cosh(\beta s)]a + [\sin(\beta s) - \sinh(\beta s)]b - e - g = 0 \\ -[\sin(\beta s) + \sinh(\beta s)]a + [\cos(\beta s) - \cosh(\beta s)]b - f - h = 0 \\ -[\cos(\beta s) + \cosh(\beta s)]a - [\sin(\beta s) + \sinh(\beta s)]b + e - g = 0 \\ \beta^3[\sin(\beta s) - \sinh(\beta s)]a - \beta^3[\cos(\beta s) + \cosh(\beta s)]b + \frac{m\omega^2}{EI}e + \beta^3 f + \frac{m\omega^2}{EI}g - \beta^3 h = 0 \end{cases} \tag{7}$$

Eq. (7) can be rewritten in the matrix form as

$$\boldsymbol{Aq} = \boldsymbol{0} \tag{8}$$

where

$$\boldsymbol{A} = \begin{bmatrix} 0 & 0 & -\beta^2\cos(\beta(L-s)) & -\beta^2\sin(\beta(L-s)) & \beta^2\cosh(\beta(L-s)) & \beta^2\sinh(\beta(L-s)) \\ 0 & 0 & \beta^3\sin(\beta(L-s)) & -\beta^3\cos(\beta(L-s)) & \beta^3\sinh(\beta(L-s)) & \beta^3\cosh(\beta(L-s)) \\ \cos(\beta s) - \cosh(\beta s) & \sin(\beta s) - \sinh(\beta s) & -1 & 0 & -1 & 0 \\ -\sin(\beta s) - \sinh(\beta s) & \cos(\beta s) - \cosh(\beta s) & 0 & -1 & 0 & -1 \\ -\cos(\beta s) - \cosh(\beta s) & -\sin(\beta s) - \sinh(\beta s) & 1 & 0 & -1 & 0 \\ \beta^3[\sin(\beta s) - \sinh(\beta s)] & -\beta^3[\cos(\beta s) + \cosh(\beta s)] & \frac{m\omega^2}{EI} & \beta^3 & \frac{m\omega^2}{EI} & -\beta^3 \end{bmatrix}$$

$$\boldsymbol{q} = [a \quad b \quad e \quad f \quad g \quad h]^T$$

By letting det($\boldsymbol{A}$) = 0, we can obtain the eigenfrequency and the mode shape of this cantilever beam with a mass.

4. Dynamics and capabilities

4.1. Frequency self-tracking range determination

To determine the excitation frequency range of our potential interest, i.e., the frequency range within which the resonance frequency changes due to the relocation of the sliding mass, the second eigenfrequency of this system is analytically derived before launching the experiment. The relationship between the second eigenfrequency of the cantilever beam and the location of the sliding mass is revealed in Fig. 4. It is noted that the second eigenfrequency can change from 52.03 Hz to 106.55 Hz, provided that the sliding mass can stop at any arbitrary location of the cantilever beam. Meanwhile, the experimental results of the mass stop position versus the excitation frequency are given in Fig. 4 to help us ascertain whether the system achieves resonance or not. In general, both results match well with each other, except that the analytical result is a bit lower than the experimental result. The potential reason for this small discrepancy is that the piezoelectric transducer is not included in the analytical modeling for simplicity, which implies that the structural stiffness is underestimated by the analytical model. Nonetheless, apart from a small discrepancy, it is experimentally proved that the excitation frequency can be tracked by the system itself, resulting in a large amplitude response over a wide frequency range.

4.2. Frequency-self-tracking energy harvesting under an invariant-frequency excitation

To illustrate the passive self-adaptation in a cantilever beam and the outstanding performance of frequency-self-tracking energy harvesting, experimental tests are conducted. Fig. 5 shows the time-history response of the voltage output and the location of the sliding mass on the cantilever beam versus the time, setting the excitation frequency to be f = 60 Hz, 65 Hz and 75 Hz respectively and the acceleration level constantly at A = 1.5 g (g is the acceleration due to gravity, i.e., 9.81 m/s^2). For the case of f = 60 Hz (as shown in Fig. 5(a)), the initial location of the sliding mass is at s = 45.5 mm and the corresponding output voltage amplitude is about 10 V. As time goes on, we observe that the sliding mass begins to move to the free end and the output voltage amplitude starts to increase in the meantime. When the sliding mass arrives at s = 64.65 mm, it stops there, like being fixed at that location of the cantilever beam. At the same moment, the output voltage attains a steady response with a constant amplitude of 29.0 V, which indicates a 290% increase as compared to the output voltage amplitude produced at the initial stage. For the case of f = 65 Hz (as shown in Fig. 5(b)), the initial location of the sliding mass is at s = 54.4 mm and the corresponding output voltage amplitude is about 2.3 V, which indicates that the vibration of the beam is very small. As time goes on, we observe that the sliding mass begins to move to the free end and stop at s = 79.65 mm, entering resonance finally. Thus, the output voltage attains a steady response with a constant amplitude of 19.0 V, which indicates an 826% increase as compared to the output voltage amplitude produced at the initial stage. For the case of f = 70 Hz (as shown in Fig. 5(c)), a similar behavior is found. The mass slides from 57.85 mm to 87 mm to match the excitation frequency, and the system finally reaches resonance. The output voltage at the large amplitude stage is 15.0 V, which is 5.818 times higher than that at the initial stage (2.2 V). Moreover, the output powers in these three cases (f = 60 Hz, 65 Hz and 75 Hz) are 7.6523 mW, 3.2848 mW, and 2.0473 mW, respectively, which are large enough to provide sustainable powers for most of the low-consumption micro-electronic devices.

Such a significant improvement of the output voltage can be explained based on the theory of resonance and off-resonance. At the initial stage, the low-level response is mainly caused by the off-resonance due to the frequency mismatch between the system's second eigenfrequency and the excitation frequency. After that, the sliding mass starts to self-tune its position, thus the eigenfrequency of the beam. As the eigenfrequency and excitation frequency approximately match, a large output voltage is achieved. This is also the reason why the mass stop positions are different under different excitation frequencies.

4.3. Frequency-self-tracking energy harvesting under a variant-frequency excitation

In practical application, the frequency of the vibration source could be variant, which requires the proposed FST-VEH to have the passively self-tuning capability to deal with the fluctuation of the excitation frequency. Thus, we would like to test

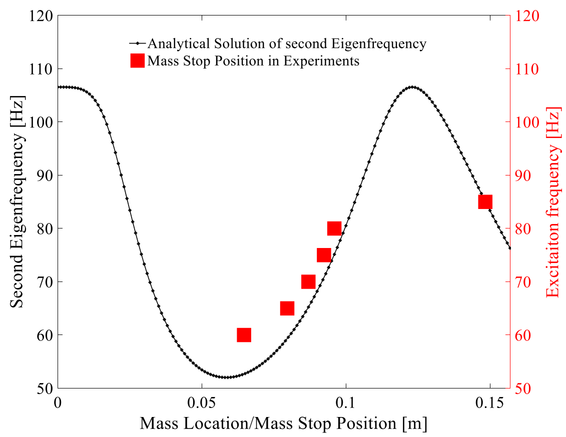

Fig. 4. Second eigenfrequency of a cantilever beam versus the mass location (line-star) and the excitation frequency versus the mass stop position (square scatters).

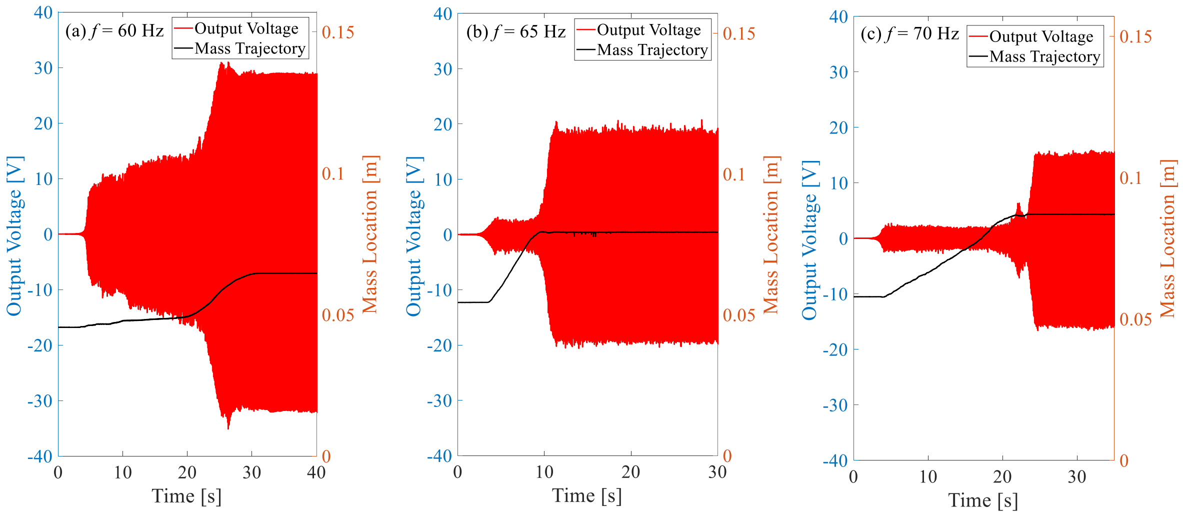

Fig. 5. Experimental results of mass trajectory and output voltage (R = 100 kΩ) when A = 1.5 g: (a) f = 60 Hz (b) f = 65 Hz (c) f = 70 Hz.

the adaptive performance of the proposed VEH when the excitation frequency suddenly changes. To this end, the acceleration of the shaker is set to be a piecewise function as:

$$A(t) = \begin{cases} 1.5\mathrm{g}\sin(2\pi \times 60t) & t \in [2.7, 25.2] \\ 0 & t \in (25.2, 32) \\ 1.5\mathrm{g}\sin(2\pi \times 65t) & t \in (32, 54.6) \\ 0 & t \in (54.6, 61.5) \\ 1.5\mathrm{g}\sin(2\pi \times 70t) & t \in [61.5, 80] \end{cases} \tag{9}$$

The frequency of the base excitation is set to be 60 Hz at the first stage, then tuned to 65 Hz and 70 Hz at the third and fifth stages, respectively. The second stage ($t\in(25.2$ s,32 s)) and the fourth stage ($t\in(54.6$ s,61.5 s)) when $A(t)$ = 0 correspond to the transition periods awaiting the change of the excitation frequency. It is worth mentioning that during the intermediate period, no additional external control is applied onto the proposed FST-VEH manually.

Fig. 6 shows the output voltage response of the proposed VEH and the trajectory of the sliding mass along the cantilever beam during the experiment. The initial position of sliding mass is at 49.15 mm. In the first stage, the mass slides to the free end and arrives at s = 64.65 mm at the end of the first stage. The output voltage increases from 14 V to 29 V, and the proposed VEH achieves a large amplitude response. During the transition stage, the voltage decreases to 0 V, and the position of the sliding mass is unchanged. At the time of 32 s, which corresponds to the beginning of the third stage, the shaker starts to generate the base excitation again with the frequency changed to f = 65 Hz. The mass gradually slides towards the free end and finally stops at s = 79.65 mm, where the whole system achieves resonance again. During this period, the voltage increases from 2.5 V to 19 V. After the second intermediate period, the shaker starts working again with the frequency changed to f = 70 Hz. At this time, the mass starts sliding and stops at s = 87 mm, where resonance is maintained again, and the voltage increases from 2.4 V to 15 V. From this experiment, it is clearly observed that even if the excitation frequency suddenly changes, the proposed VEH can autonomously calibrate the natural frequency through relocating the sliding mass to match the excitation frequency for maintaining resonance by itself.

In summary, it is a remarkable fact that in the whole process of the experiments, the proposed system exhibits a self-adaptive behavior by autonomously calibrating its natural frequency to track the excitation frequency of the vibration source without any manual intervention. As a result, even when the excitation frequency changes a lot, the system can achieve resonance and maintain a large output voltage, which is very promising to efficiently harvest variant-frequency vibration energy. All these results can be found in the experimental videos recorded by the high-speed camera (Supplementary materials).

5. Mode shape reconstruction and energy harvesting performance

5.1. Mode shape reconstruction

To ascertain the underlying mechanism behind the passively self-adaptive behavior, the vibrating shape of the system is captured experimentally using the high-speed camera. The analytical mode shape of a cantilever beam with a position-fixed mass is calculated to assist the identification of the characteristics of the experimentally obtained vibrating shape. It is worth

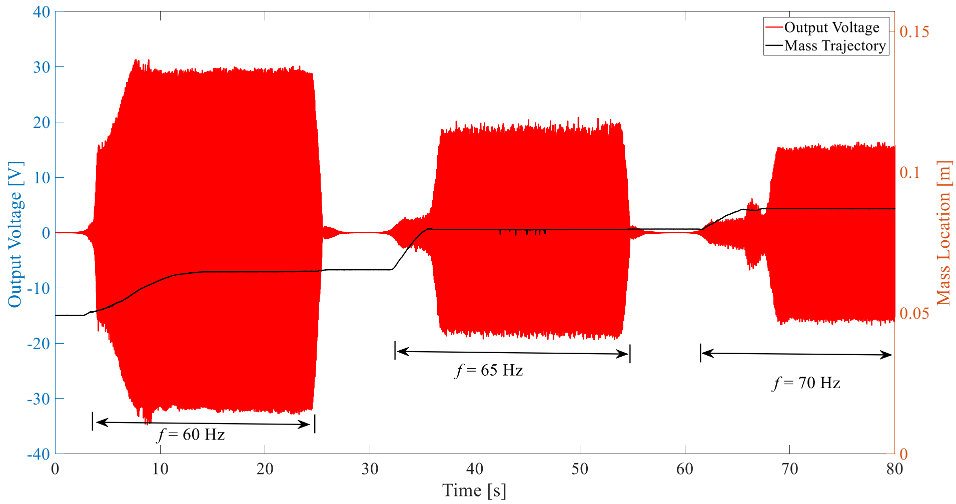

Fig. 6. Experimental results of the time histories of mass location and output voltage when excitation frequency f shifts from 60 Hz to 65 Hz and finally reaches 70 Hz (A = 1.5 g, R = 100 kΩ).

mentioning that for the cases under high-frequency excitations, the vibrating shape cannot be clearly recognized based on just a single frame of motion captured by the high-speed camera. To overcome this problem, we select two very close frames of motion and put them together in a single plot to help recognize the nodes and antinodes of the vibrating shapes.

Fig. 7 shows the vibrating shapes of the system under different excitation frequencies and the analytical second-order mode shapes of a cantilever beam with the same mass being fixed at the corresponding stop positions measured from the experiment. It is noted that experimentally captured vibrating shapes and the analytical mode shapes agree very well. A minor difference is that the experimentally captured vibrating shapes are slightly tilted due to gravity, which is not considered in the analytical model. Notably, it is clearly shown in the images captured by the high-speed camera that the mass

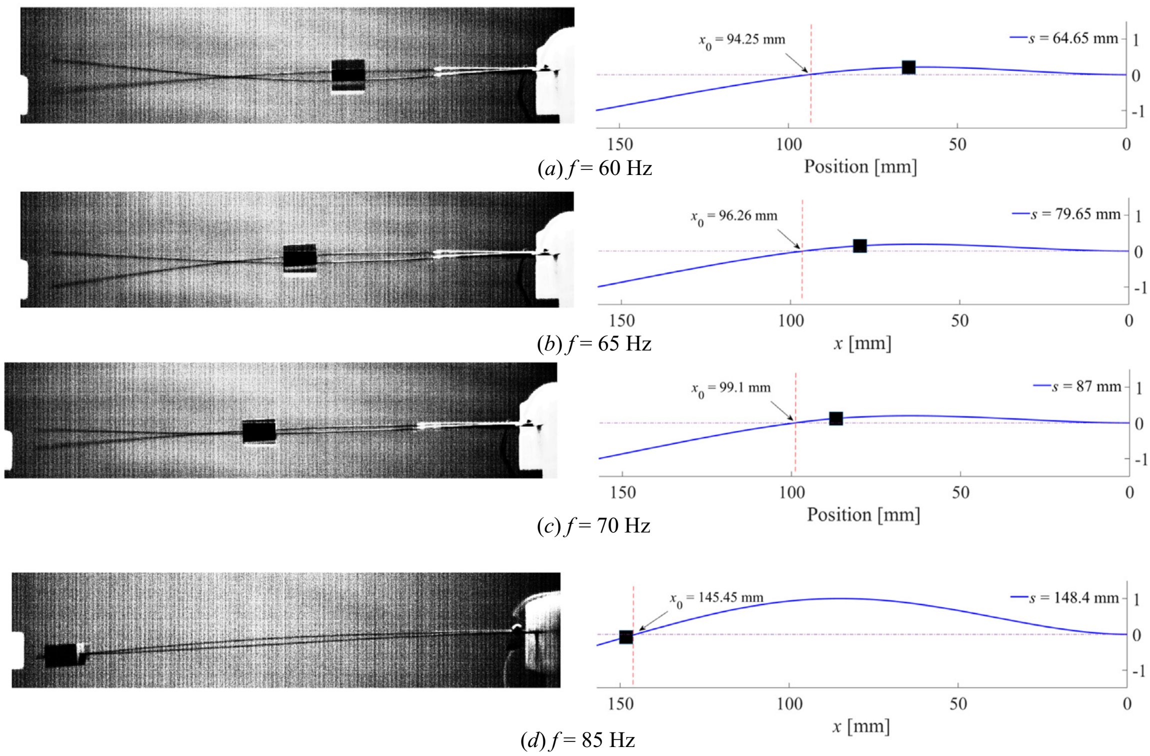

Fig. 7. Experimental vibrating shape (left) and analytical mode shape (right) for various excitations: (a) f = 60 Hz; (b) f = 65 Hz; (c) f = 70 Hz;(d) f = 85 Hz.

stop positions are not at the node nor antinode of the second mode shape. Meanwhile, it is clearly shown in Fig. 7 that the mass stop position varies with the change of the excitation frequency, and the mode shape of the proposed FST-VEH is correspondingly reconstructed. For the excitation frequencies f = 60 Hz, f = 65 Hz, f = 70 Hz, and f = 85 Hz, the mass stop positions are s = 64.65 mm, s = 79.65 mm, s = 87 mm, and s = 148.4 mm, respectively. When the stop positions of the sliding mass are different, the corresponding mode shapes and vibrating shapes are also different. Though it might be difficult to affirm by directly comparing the mode shape curves, we can compare their mode shape nodes. Under the excitation frequencies of f = 60 Hz, f = 65 Hz, and f = 70 Hz, the mode shape nodes are at 94.25 mm, 96.26 mm, and 99.1 mm, respectively. To give a high-contrast comparison, one can refer to the result of f = 85 Hz (i.e., Fig. 7(d)). As compared to other cases (i.e., Fig. 7(a)-(c)), it is obvious that the mode shape and vibrating shape for the case of f = 85 Hz are quite different based on even a naked-eye comparison. Hence, it can be concluded that the change of the excitation frequency will lead to the mode shape reconstruction, which enables the proposed FST-VEH to autonomously track the excitation frequency of the vibration source and maintain resonance to improve the energy harvesting efficiency.

As the mode shape reconstruction is confirmed to be induced by the mass sliding behavior, the underlying physics behind the whole frequency-self tracking process (i.e., the mass sliding process) can be explained as follow. In the beginning, when the beam-slider system starts to vibrate under the external excitation, the mass will start to slide along the cantilever beam if the friction force is lower than the tractive force. Notably, if the beam's vibration response is very weak, the friction force could be larger than the tractive force. In this case, the mass acts as a fixed mass. Hence, the vibration response of the beam and mass should exceed a certain level to ensure that the mass can slide along the beam. However, if the beam's vibration response is very large, the initial force of the mass could be very large, result in a large friction force. In this case, the friction force is possible to balance the tractive force along the beam and stop the sliding mass at a certain position. Hence, the friction force plays a significant role in affecting the passively self-adaptive behavior. Since the weight ratio of the mass to the cantilever beam is quite large, the change of the mass location can profoundly affect the mode shape of the entire system (e.g., mode shape reconstruction). As a result, the eigenfrequencies of the entire system are closely dependent on the location of the sliding mass. In the process of sliding, the force component endured by the sliding mass in parallel with the beam length direction drives it to slide, while the friction force between the mass and beam plays the role of a resistive force to stop it. This friction force is directly proportional to the force component endured by the sliding mass normal to the beam surface, which is dependent on the inertial force of the sliding mass. Hence, the friction force is closely relevant to the vibration intensity of the sliding mass. Suppose that the eigenfrequency of the beam-slider system is far away from the excitation frequency at the initial stage, the entire beam-slider system is at off-resonance with a relatively low vibration intensity. As a result, the friction force is small, and the mass starts to slide on the beam. The mass thus continuously changes its location, and the eigenfrequency of the beam-slider system approaches the excitation frequency. In this process, the entire system gradually becomes near/on-resonance from off-resonance. In the meantime, the inertia of the sliding mass largely increases, and thus the friction force. When the friction force becomes sufficiently large to balance the force component endured by the sliding mass in parallel with the beam length direction, the mass will eventually stop. This is the most likely reason to explain why the mass starts to slide along the beam when the eigenfrequency and excitation frequency differ a lot from each other, and why the mass stops at a certain place with a large amplitude response when the eigenfrequency and excitation frequency are very close. Since it cannot be guaranteed that the force balance will take place when the mass just slides to a place where the eigenfrequency of the beam-slider completely matches the excitation frequency, the entire system may finally falls into only near-resonance.

5.2. Energy harvesting performance

To further illustrate the advantages of the proposed FST-VEH, its power performance is compared to that of a conventional VEH having the mass fixed at certain places (s = 71 mm, s = 83.6 mm, and s = 85 mm). The mass in the FST-VEH configuration is allowed to move freely along the beam. In the experiment, the load resistance is kept 100 kΩ for both the proposed FST-VEH and the conventional VEH configurations for a fair comparison. A frequency sweep experiment was first conducted to obtain the power-frequency response of the conventional VEH. A frequency dwelling experiment was then performed at a series of discrete frequencies to obtain the power-frequency relation of the proposed FST-VEH. It is learned from Fig. 8 that when the mass is fixed at a certain place, the mass-beam system acts as a conventional VEH with a relatively narrow working frequency band. For example, we compare the power outputs of the proposed FST-VEH and the conventional VEH with the mass fixed at s = 83.6 mm. Assuming the threshold power (i.e., the minimum power demand for practical application) is 1 mW, the operational bandwidth of the conventional VEH (s = 83.6 mm) is only about 2.08 Hz. It is noteworthy that the frequency response curve of the conventional VEH exhibits a jumping phenomenon near the resonance. The main reason is that the geometric nonlinearity is induced due to the large deformation of the slender beam near the resonance. Regarding the proposed FST-VEH, it can produce a power output larger than 1 mW over the frequency range from 63 Hz to 74 Hz. Thus, the bandwidth of the proposed FST-VEH is at least more than 11 Hz, which indicates an improvement of 428.8% as compared to the conventional VEH (s = 83.6 mm).

In terms of the maximum power output, it is found that the conventional VEH produces a larger output power than the proposed FST-VEH only when the resonance takes place. There are mainly two potential reasons that can be used to explain the decrease in the power of the proposed FST-VEH. The first one is that the collision-sliding behavior between the sliding mass and cantilever beam possibly consumes additional kinetic energy, leading to the reduction of the dynamic response

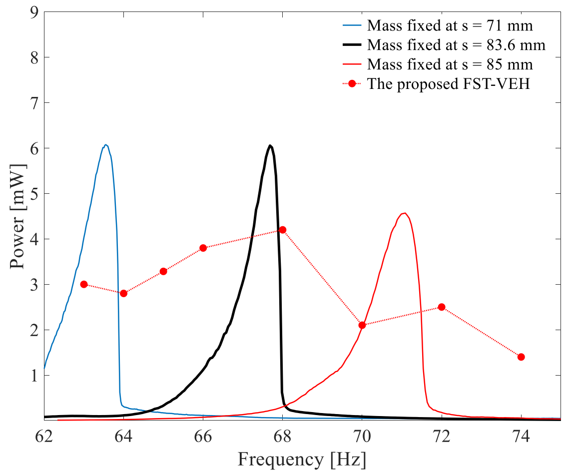

Fig. 8. Experimental comparison of the generated power of the FST-VEH and the conventional VEH (A = 1.5 g).

and the power output. The second one is that the second eigenfrequency of the proposed FST-VEH might have not been perfectly self-adjusted to the excitation frequency. For a linear VEH, a minor derivation from the resonance frequency can significantly reduce the output power. Fortunately, from the experimental results, the generated power of the proposed FST-VEH is kept at a relatively high level over a wide frequency range.

Generally speaking, the most attractive feature of the proposed FST-VEH is not the ability to significantly increase the energy harvesting efficiency near one particular frequency, but the capability of improving the power level over a wide frequency range, within which the conventional VEH is at off-resonance and out of service. For example, at f = 70 Hz, the generated power of the conventional VEH (s = 83.6 mm) is only 0.086 mW, while that of the proposed FST-VEH is 2.1 mW. Moreover, at f = 64 Hz, the power outputs of the proposed FST-VEH and the conventional VEH (s = 83.6 mm) are 2.8 mW and 0.115 mW, respectively. Similar performance enhancements are also observed at other frequencies, indicating an extremely broadband capability of the proposed FST-VEH. Therefore, it is convinced that, owing to its exceptional frequency-self-tracking feature, the proposed FST-VEH can adapt to excitation frequency changes and significantly improve vibration energy harvesting efficiency over a broad frequency range. Therefore, it is a viable and promising solution to overcome the challenge of variant-frequency vibration energy harvesting in practical scenarios.

6. Conclusions

This paper has reported the discovery of a passively self-adaptive cantilever beam with a sliding mass. It represents a first observation of the passive self-adaptative phenomenon in the asymmetric structure. The passive self-adaptative phenomenon has been found to take place at the second eigenmode rather than the fundamental eigenmode. The mode shape reconstruction is clearly observed to help ascertain the mechanism of frequency-self-tracking. Since the cantilever beam is widely used in designing both linear and nonlinear VEHs, this passively self-adaptative structure is promising to overcome some of the most severe limitations of conventional VEHs, such as efficiently and robustly harvesting energy from the broadband and variant-frequency vibration environments. The unique behavior of the proposed energy harvesting system has been experimentally proved to help self-track the frequencies of vibration sources and significantly improve the output power over a wide range of frequencies. For the prototyped system tested in the experiment, the working bandwidth has been increased at least by 428.8%, and the power output has been increased at most by 24.4 times.

CRediT authorship contribution statement

Chunbo Lan: Conceptualization, Data curation, Formal analysis, Funding acquisition, Investigation, Methodology, Supervision, Validation, Writing - original draft. **Zhenning Chen:** Data curation, Investigation, Validation, Writng - review & editing. **Guobiao Hu:** Methodology, Investigation, Writing - review & editing. **Yabin Liao:** Investigation, Writing - review & editing. **Weiyang Qin:** Supervision, Funding acquisition.

Declaration of Competing Interest

The authors declare that they have no known competing financial interests or personal relationships that could have appeared to influence the work reported in this paper.

Acknowledgment

This study was supported by Natural Science Foundation of China (Grant No. 11672237, 12002152), Natural Science Foundation of Jiangsu Province (Grant No. BK20190379), China Postdoctoral Science Foundation Funded Project (Grant No.2020 M681577) and a project funded by the Priority Academic Program Development of Jiangsu Higher Education Institutions.

Data availability statement

The data that support the findings of this study are available from the corresponding author upon reasonable request.

Appendix A. Supplementary data

Supplementary data to this article can be found online at https://doi.org/10.1016/j.ymssp.2021.107672.

References

[1] A. Erturk, D.J. Inman, Piezoelectric energy harvesting, John Wiley & Sons, 2011.
[2] H. Liu, J. Zhong, C. Lee, S.W. Lee, L. Lin, A comprehensive review on piezoelectric energy harvesting technology: materials, mechanisms, and applications, Appl. Phys. Rev. 5 (2018) 041306.
[3] X. Zhang, J. Grajal, J.L. Vazquez-Roy, U. Radhakrishna, X. Wang, W. Chern, L. Zhou, Y. Lin, P.C. Shen, X. Ji, X. Ling, Two-dimensional MoS 2-enabled flexible rectenna for Wi-Fi-band wireless energy harvesting, Nature 566 (2019) 368.
[4] C. Wei, X. Jing, A comprehensive review on vibration energy harvesting: modelling and realization, Renew. Sustain. Energy Rev. 74 (2017) 1–18.
[5] Z. Yang, S. Zhou, J. Zu, D. Inman, High-performance piezoelectric energy harvesters and their applications, Joule 2 (2018) 642–697.
[6] K. Fan, H. Qu, Y. Wu, T. Wen, F. Wang, Design and development of a rotational energy harvester for ultralow frequency vibrations and irregular human motions, Renew. Energy 156 (2020) 1028–1239.
[7] D. Castagnetti, F. Dallari, Design and experimental assessment of an electromagnetic energy harvester based on slotted disc springs, P. I. Mech. Eng. L-J. Mat. 231 (2017) 89–99.
[8] D. Castagnetti, Fractal-inspired multifrequency structures for piezoelectric harvesting of ambient kinetic energy, ASME. J. Mech. Des. 133 (11) (2011) 111005.
[9] S.C. Stanton, C.C. McGehee, B.P. Mann, Reversible hysteresis for broadband magnetopiezoelastic energy harvesting, Appl. Phys. Lett. 95 (2009) 174103.
[10] A. Erturk, J. Hoffmann, D.J. Inman, A piezomagnetoelastic structure for broadband vibration energy harvesting, Appl. Phys. Lett. 94 (2009) 254102.
[11] F. Cottone, H. Vocca, L. Gammaitoni, Nonlinear energy harvesting, Phys. Rev. Lett. 102 (2009) 080601.
[12] S. Zhou, J. Cao, D.J. Inman, J. Lin, S. Liu, Z. Wang, Broadband tristable energy harvester: modeling and experiment verification, Appl. Energy 133 (2014) 33–39.
[13] W. Liu, Z. Yuan, S. Zhang, Q. Zhu, Enhanced broadband generator of dual buckled beams with simultaneous translational and torsional coupling, Appl. Energy 251 (2019) 113412.
[14] L. Chen, W. Jiang, Internal resonance energy harvesting, J. Appl. Mech-T. ASME. 82 (2015) 031004.
[15] H. Liu, C. Lee, T. Kobayashi, C.J. Tay, C. Quan, Investigation of a MEMS piezoelectric energy harvester system with a frequency-widened-bandwidth mechanism introduced by mechanical stoppers, Smart Mater. Struct. 21 (2012) 035005.
[16] C. Lan, W. Qin, Enhancing ability of harvesting energy from random vibration by decreasing the potential barrier of bistable harvester, Mech. Syst. Signal Pr. 85 (2017) 71–81.
[17] Z. Yuan, W. Liu, S. Zhang, Bandwidth broadening through stiffness merging using the nonlinear cantilever generator, Mech. Syst. Signal Pr. 132 (2019) 1–17.
[18] Y. Wang, X. Jing, Nonlinear stiffness and dynamical response characteristics of an asymmetric X-shaped structure, Mech. Syst. Signal Pr. 125 (2019) 142–169.
[19] W. Wang, J. Cao, D. Mallick, S. Roy, J. Lin, Comparison of harmonic balance and multi-scale method in characterizing the response of monostable energy harvesters, Mech. Syst. Signal Pr. 108 (2018) 252–261.
[20] M.F. Daqaq, R. Masana, A. Erturk, D.D. Quinn, On the role of nonlinearities in vibratory energy harvesting: a critical review and discussion, Appl. Mech. Rev. 66 (2014) 040801.
[21] A. Erturk, D.J. Inman, Broadband piezoelectric power generation on high-energy orbits of the bistable Duffing oscillator with electromechanical coupling, J. Sound Vib. 330 (2011) 2339–2353.
[22] L. Yu, L. Tang, L. Xiong, T. Yang, Capture of high energy orbit of Duffing oscillator with time-varying parameters, Chaos 30 (2020) 023106.
[23] L. Yan, M. Lallart, A. Karami, Low-cost orbit jump in nonlinear energy harvesters through energy-efficient stiffness modulation, Sensor. Actuat. A: Phys. 285 (2019) 676–684.
[24] T. Huguet, M. Lallart, A. Badel, Orbit jump in bistable energy harvesters through buckling level modification, Mech. Syst. Signal Pr.128 (2019) 202–215.
[25] G. Sebald, H. Kuwano, D. Guyomar, B. Ducharne, Experimental Duffing oscillator for broadband piezoelectric energy harvesting, Smart Mater. Struct. 20 (2011) 102001.
[26] D. Mallick, A. Amann, S. Roy, Surfing the high energy output branch of nonlinear energy harvesters, Phys. Rev. Lett. 117 (2016) 197701.
[27] C. Lan, L. Tang, W. Qin, Obtaining high-energy response of nonlinear piezoelectric energy harvester by voltage impulse perturbation, Eur. Phys. J. Appl. Phys. 79 (2017) 20902.
[28] J. Wang, W. Liao, Attaining the high-energy orbit of nonlinear energy harvesters by load perturbation, Energy Convers. Manage. 192 (2019) 30–36.
[29] A. Pasharavesh, M.T. Ahmadian, Toward wideband piezoelectric harvesters through self-powered transitions to high-energy response, J. Vib. Acoust. 142 (2020) 011021–11031.
[30] A. Boudaoud, Y. Couder, M.B. Amar, Self-adaptation in vibrating soap films, Phys. Rev. Lett. 82 (1999) 3847.
[31] M. Brazovskaia, P. Pieranski, Self-tuning behavior of vibrating smectic films, Phys. Rev. Lett. 80 (1998) 5595.
[32] A. Boudaoud, Y. Couder, M.B. Amar, A self-adaptative oscillator, Eur. Phys. J. B. 9 (1999) 159–165.
[33] L.M. Miller, P. Pillatsch, E. Halvorsen, P.K. Wright, E.M. Yeatman, A.S. Holmes, Experimental passive self-tuning behavior of a beam resonator with sliding proof mass, J. Sound Vib. 332 (2013) 7142–7152.
[34] L.M. Miller, Micro-scale piezoelectric vibration energy harvesting: from fixed-frequency to adaptable-frequency devices, UC Berkeley (2012).
[35] M. Krack, N. Aboulfotoh, J. Twiefel, J. Wallaschek, L.A. Bergman, A.F. Vakakis, Toward understanding the self-adaptive dynamics of a harmonically forced beam with a sliding mass, Arch. Appl. Mech. 87 (2017) 699–720.
[36] L. Yu, L. Tang, T. Yang, Experimental investigation of a passively self-tuning resonator based on a beam-slider structure, ACTA Mech. Sinica. 35 (2019) 1079–1092.

[37] J.L. Kaplan, P. Bonello, M. Alalwan, A simulation of the performance of a self-tuning energy harvesting cantilever beam, J. Phys.: Conf. Ser. 744 (2016) 012083.

[38] M.G. Scirè, D. Castagnetti, E. Dragoni, Closed-form modal analysis of flexural beam resonators ballasted by a rigid mass, P. I. Mech. Eng. L-J. Mat. 230 (3) (2016) 717–734.